

# Electron Ageing and Polarization in Tailed Radio Galaxies

L. Feretti<sup>1</sup>, G. Giovannini<sup>1,2</sup>, U. Klein<sup>3</sup>, K.-H. Mack<sup>1,3</sup>, L.G. Sijbring<sup>4</sup>, and G. Zech<sup>3</sup>

<sup>1</sup> Istituto di Radioastronomia del CNR, Via P. Gobetti 101, I-40129 Bologna, Italy

<sup>2</sup> Dipartimento di Astronomia, Università di Bologna, Via Zamboni 33, I-40126 Bologna, Italy

<sup>3</sup> Radioastronomisches Institut der Universität Bonn, Auf dem Hügel 71, D-53121 Bonn, Germany

<sup>4</sup> Kapteyn Astronomical Institute, Postbus 800, NL-9700 AV Groningen, The Netherlands

April 6, 2018

**Abstract.** High-frequency observations of the tailed radio galaxies IC 310, NGC 1265, 3C 129, and 3C 465 have been performed with the Effelsberg 100-m telescope. For the radio galaxies IC 310, NGC 1265 and 3C 465, radio data obtained at low frequencies with the Westerbork Synthesis Radio Telescope are also available. These new radio data allow us to map the extended structure of the radio galaxies and obtain spectral and polarization information in the outermost regions.

The multi-frequency spectra were used to study the synchrotron ageing of relativistic electrons with increasing distance from the active nucleus. We found that the spectrum in each radio galaxy progressively steepens with distance, and at each location it is steeper at high frequencies. The spectra are fitted by models involving synchrotron energy losses and the critical frequency is obtained at increasing distance from the core. Assuming that the magnetic field is the equipartition value, we obtain the radiating electron lifetimes and consequently their drift velocities. Our results imply the existence of reacceleration processes or bulk motions along the tails.

The polarization data at 10.6 GHz give information on the intrinsic degree of polarized flux and the orientation of the magnetic field. We find that the polarization percentage increases along the tails, reflecting an increase of the degree of ordering of the magnetic field. The magnetic field in the tails is longitudinal.

**Key words:** Galaxies: individual: IC 310, NGC 1265, 3C 129, 3C 465 – Galaxies: magnetic fields – Radio continuum: galaxies

## 1. Introduction

The study of extended radio galaxies in clusters of galaxies is important to understand the evolution of radio sources. In particular, the low-brightness lobes are at a late stage of evolution and are typically confined by the intergalactic medium, therefore synchrotron losses dominate in these regions. Studies of extended radio sources often suffer from limitations of the high-resolution interferometric observations, which can properly map the low-brightness regions only at low frequencies (610 – 327 MHz or lower). On the other hand, information on the relativistic particle ageing and on the polarization behaviour of the extended low-brightness regions is only obtained with multiple frequencies.

The Effelsberg 100-m radio telescope is at present the best available instrument to map the outermost regions of extended radio galaxies with good angular resolution, overcoming the problem of the lack of short spacings (see e.g. Andernach et al. 1992 and Mack et al. 1993). Thanks to its high sensitivity, it is possible to map the extended structures at 10.6 GHz. At this high frequency, Faraday effects are generally negligible, thus the intrinsic degree of polarization and the orientation of magnetic field can be derived. Moreover, energy losses in relativistic electrons are severely affecting the emission spectrum, allowing a determination of the particle ageing at different distances from the core.

In this paper we present new multi-frequency radio data of the extended tailed radio galaxies IC 310, NGC 1265, 3C 129, and 3C 465, revealing the spectral index trends and the polarization behaviour up to the outermost regions. The spectral steepening can thence be used to determine the particle ages, following e.g. the procedure of Carilli et al. (1991). Tailed radio sources are particularly suited for this purpose. In fact, according to currently accepted models, the morphology of these sources is affected by the drag action exerted by the intergalactic medium on the moving galaxy, and the low-brightness tails consist of

aged relativistic electrons, which have reached pressure equilibrium with the ambient gas and are losing energy essentially through synchrotron radiation and the inverse Compton effect. Since the radio emitting electrons are expected to be older at greater distance from the nucleus, the variation of the physical conditions with distance is related to the time evolution of the radio plasma.

In Sect. 2 we briefly describe the observations and data reduction techniques. Section 3 presents the results, which are discussed in Sect. 4, with emphasis on the particle lifetime and velocity, and the magnetic field morphologies. In Sect. 5 we summarize our results and present our conclusions. A Hubble constant  $H_0 = 100 \text{ km s}^{-1} \text{ Mpc}^{-1}$  and a  $q_0 = 1$  are assumed.

## 2. Observations and data analysis

The observations at 10.6, 4.8, and 2.7 GHz have been carried out using the 100-m radio telescope at Effelsberg. In Table 1 we have listed the radio galaxies, together with their position and redshift, the observing frequency, the angular resolution in the final maps, the r.m.s. noise level in the I and U, Q maps.

Fields were mapped in azimuth and elevation (see Emerson et al. 1979 for details) for each source ensuring sufficiently large areas to also account for the beam throws involved. The number of coverages and field sizes for each source are given in Table. 1. The 2.7-GHz map of 3C 129 was obtained by scanning in right ascension and declination 30 times, as this receiver has a single feed so that mapping in Az-El is not mandatory. At the two highest frequencies, difference maps were obtained to remove atmospheric fluctuations in the signals and the conventional restoration technique of Emerson et al. (1979) was applied. The resulting Stokes I, U, and Q maps were subsequently transformed into the equatorial coordinate system, and individual coverages finally averaged (with weights proportional to the inverse squares of the rms noise values). Maps at 10.6 GHz were finally CLEANed, with the algorithm described by Klein & Mack (1995). Calibration of the flux density scale and the polarization parameters was achieved by frequently cross-scanning and mapping the point sources 3C 48, 3C 138, 3C 286, and 3C 295, with the flux density scale adopted from Baars et al. (1977).

For the radio galaxies IC 310 and NGC 1265, maps at 610 and 327 MHz were extracted from the image of the Perseus cluster (Sijbring 1993), obtained with the Westerbork Synthesis Radio Telescope (WSRT). The shortest baseline at both frequencies was 36 m, therefore only structures larger than  $48'$  at 610 MHz and  $1^{\circ}4$  at 327 MHz are missed. This ensures that these measurements are not affected by the lack of short baselines, and a comparison between Effelsberg and WSRT data is possible. Similarly, the WSRT map of the radio galaxy 3C 465, obtained by Jägers (1987) with the WSRT at 610 MHz, was used in the present work. The WSRT maps, available only in total in-

tensity, were convolved to the resolution of the Effelsberg maps.

The images were analyzed with the AIPS package. To compare observations of the same source at different frequencies we convolved all the maps to the lowest resolution with a gaussian. Thereafter, the maps were re-gridded by means of the task 'HGEOM' in AIPS to have identical pixel size.

## 3. Results

### 3.1. IC 310 - 0313+411

IC 310 is located in the Perseus cluster. Previous observations of this radio galaxy are listed by Mack et al. (1993), who first mapped the large-scale structure of this source at a high frequency. The 10.6-GHz map presented here in Fig. 1 has a higher sensitivity, owing to additional scans. For the spectral comparison, we used the WSRT maps at 327 and 610 MHz by Sijbring (1993), convolved to the same resolution of  $69''$ .

The trend of the spectral index ( $\alpha_{0.3}^{0.6}$  and  $\alpha_{0.6}^{10.6}$ ;  $I_\nu \propto \nu^{-\alpha}$ ) derived along the maximum brightness ridge is given in Fig. 5. The low-frequency spectral index  $\alpha_{0.3}^{0.6}$  is 0.4, almost constant up to  $2'$  from the core, suggesting that the particles radiating in this region and at low frequencies have not suffered synchrotron losses. A clear steepening is visible at high frequencies and with increasing distance from the core.

The tail is strongly polarized, up to a distance of  $3'$  from the core, with the polarization percentage increasing along the tail (see Fig. 6). The orientation of the polarization vectors is perpendicular to the tail (see Fig. 1).

### 3.2. NGC 1265 - 0314+416

NGC 1265 is located in a peripheral region of the Perseus Cluster, at about  $27'$  north-west of the active galaxy NGC 1275 (3C 84). Previous studies of this source are listed in Mack et al. (1993), who obtained the first image at 10.6 GHz. The 10.6-GHz map presented here (Fig. 2) has a much higher sensitivity than that of Mack et al. (1993), owing to a longer observing time. We also obtained observations at 4750 MHz and extracted WSRT maps at 327 and 610 MHz from the Perseus Cluster image obtained by Sijbring (1993). We note that the very-low-brightness feature first reported by Gisler & Miley (1979) and observed with higher sensitivity and dynamic range by Burns et al. (1992) and by Sijbring (1993) is just indicated in our 10.6-GHz map if smoothed to a  $1.5$  beam, especially in the (more sensitive) map of linear polarization. At the other frequencies the feature, if present, is concealed by the sidelobe structure which we could not yet clean at this wavelength.

All maps were smoothed to the common resolution of  $147''$  for a multifrequency comparison. The trend of the spectral index along the ridge of maximum brightness for

**Table 1.** Radio sources and observational details

Source	RA(B1950) [ h m s]	DEC(B1950) [ ° ' '' ]	z	Freq. [MHz]	# Cov.	Map size	HPBW [']	$\sigma_I$ [mJy/beam]	$\sigma_{U,Q}$ [mJy/beam]
IC310	03 13 25.2	41 08 30	0.0183	327	-	-	69	3.2	-
				610	-	-	69	0.4	-
				10550	12	29' × 8'	69	0.5	0.3
NGC1265	03 14 56.8	41 40 32	0.0183	327	-	-	147	5.1	-
				610	-	-	147	0.3	-
				4750	13	28' × 20'	147	5.0	2.5
				10550	22	35' × 14'	69	0.6	0.5
3C129	04 45 21.0	44 56 48	0.021	2695	30	40' × 26'	258	4.4	3.3
				4750	30	35' × 17'	147	3.4	1.5
				10550	21	46' × 25'	69	1.0	0.4
3C465	23 35 59.0	26 45 16	0.0322	610	-	-	147	5.0	-
				4750	11	26' × 18'	147	2.3	1.3
				10550	20	35' × 14'	69	0.9	0.5

the 3 frequency pairs is presented in Fig. 5. Between 0.3 and 4.8 GHz it is in the range 0.5 – 0.8, while beyond 4.8 GHz a strong steepening is evident, which increases with distance from the core, reaching a value  $\alpha > 2$  at the tail's end.

Strong linear polarization is found in the external tail region (see Fig. 6). The polarization percentage at 10.6 GHz increases along the tail up to  $\sim 40\%$ . At 4.8 GHz, the degree of polarization is comparable to that at 10.6 GHz up to 5' from the core, and is lower beyond that distance. The electric vector at both frequencies is perpendicular to the tail orientation.

### 3.3. 3C129

This radio source is identified with an E galaxy in the galactic plane ( $l_{II}=160.4^\circ$ ,  $b_{II}=0.1^\circ$ ). It was studied by many authors (e.g. Miley 1973, Rudnick & Burns 1981, Van Breugel 1982, Van Breugel & Jägers 1982) with interferometric observations. The Effelsberg map at 10.6 GHz is given in Fig. 3. Maps were also obtained at 2.7 GHz and 4.8 GHz. The tail of this source, which at lower frequencies is about 30' long (Van Breugel 1982), is detected out to about 20' at 2.7 GHz and to about 12' at 10.6 GHz.

The spectral index along the source was obtained with an angular resolution of about 4' (Fig. 5). The spectrum strongly steepens from the core to the outer regions, reaching values up to  $\alpha \sim 3$ . The polarization percentage (Fig. 6) in the outermost tail region reaches values of  $\sim 60\text{--}70\%$  at high frequencies and is slightly lower at 2.7 GHz. The polarization vector at 10.6 GHz is perpendicular to the tail, and shows significant rotation at lower frequencies.

### 3.4. 3C465

This source is identified with a cD galaxy at the centre of the rich cluster A2634. It is the prototype of wide-angle tailed radio sources (see e.g. Eilek et al. 1984 and references therein), and a model of its dynamical evolution has been proposed by Leahy (1984). High-resolution VLA maps show an unresolved core, and two asymmetric jets which terminate in a bright spot and after a sharp bending, in extended lobes. In our maps at 4.8 GHz (not shown here) and 10.6 GHz (Fig. 4), both the N-S and E-W tails are well resolved. We derived the point-to-point spectrum in the tails, with an angular resolution of 147'', using also the 610 MHz WSRT map of Jägers (1987).

The spectral index between 0.6 and 4.8 GHz is lower than that between 4.8 and 10.6 GHz, except for the outermost points of the N-S lobe, where however the two values are consistent within the errors. A remarkable high-frequency steepening is present in the E-W lobe, at increasing distance from the core (Fig. 5). The polarization percentage at both 10.6 and 4.8 GHz is asymmetric and is higher in the N-S lobe (Fig. 6).

## 4. Discussion

### 4.1. Evolution of the spectrum along the sources

The spectral behaviour in all the sources presented here is similar. The spectrum between two given frequencies shows a progressive steepening with increasing distance from the core. Moreover, the steepening is stronger in the high-frequency range than at lower frequencies. Since the radio emitting electrons are expected to be older at larger distance from the core, the variation of the spectrum with distance is related to its evolution with time under the effect of radiation losses.

**Table 2.** Critical frequencies, electron lifetimes and projected velocities for IC 310 with  $\gamma = 1.8$ 

Distance [']	$\nu_c$ (KP) [GHz]	$\nu_c$ (JP) [GHz]	$H_{\text{eq}}$ [ $\mu$ G]	Age(KP) [ $\times 10^7$ yr]	Age(JP) [ $\times 10^7$ yr]	Vel(KP) [100 km s $^{-1}$ ]	Vel(JP) [100 km s $^{-1}$ ]
0.5	>30.0	>30.0	4.3	<2.0	<2.0	>3.8	>3.8
1.0	>30.0	>30.0	3.6	<2.2	<2.2	>6.9	>6.9
1.5	30.0	23.9	3.3	2.4	2.6	9.6	8.6
2.0	12.1	10.3	3.3	3.7	4.0	5.6	5.5
2.5	5.5	5.6	3.1	5.7	5.6	3.9	4.8
3.0	3.6	4.5	3.1	6.9	6.2	5.9	12.0
3.5	2.2	1.8	2.9	9.2	10.3	3.4	1.9
4.0	1.7	1.4	2.8	10.5	11.7	5.8	5.4
4.5	1.2	1.0	2.7	12.7	13.9	3.4	3.4
5.0	0.7	0.6	2.3	17.5	18.2	1.6	1.8
5.5	0.4	0.5	2.2	21.8	21.1	1.8	2.6
6.0	0.3	0.4	1.9	25.7	22.7	1.9	4.7

**Table 3.** Critical frequencies, electron lifetimes and projected velocities for NGC 1265 with  $\gamma = 2.2$ 

Distance [']	$\nu_c$ (KP) [GHz]	$\nu_c$ (JP) [GHz]	$H_{\text{eq}}$ [ $\mu$ G]	Age(KP) [ $\times 10^7$ yr]	Age(JP) [ $\times 10^7$ yr]	Vel(KP) [100 km s $^{-1}$ ]	Vel(JP) [100 km s $^{-1}$ ]
1	>30.0	>30.0	3.5	<2.3	<2.3	>6.6	>6.6
2	>30.0	26.0	3.5	<2.3	2.5	>13.2	12.3
3	17.6	14.5	3.2	3.1	3.4	14.6	15.4
4	12.9	11.0	3.1	3.7	4.0	26.5	26.9
5	10.9	9.5	3.1	4.0	4.3	45.7	50.3
6	9.1	8.2	3.0	4.4	4.7	35.1	38.7
7	7.8	7.2	2.9	4.9	5.1	35.9	39.7
8	6.5	6.2	2.7	5.5	5.6	25.6	29.0
9	5.5	5.3	2.6	6.0	6.1	28.5	29.6
10	4.8	4.6	2.3	6.6	6.7	26.5	25.1

**Table 4.** Critical frequencies, electron lifetimes and projected velocities for 3C 129 with  $\gamma = 2.4$ 

Distance [']	$\nu_c$ (KP) [GHz]	$\nu_c$ (JP) [GHz]	$H_{\text{eq}}$ [ $\mu$ G]	Age(KP) [ $\times 10^7$ yr]	Age(JP) [ $\times 10^7$ yr]	Vel(KP) [100 km s $^{-1}$ ]	Vel(JP) [100 km s $^{-1}$ ]
1	>30.0	>30.0	4.1	<2.1	<2.1	>8.4	>8.4
2	>30.0	>30.0	3.9	<2.1	<2.1	>16.2	>16.2
3	>30.0	>30.0	4.2	<2.0	<2.0	>25.6	>25.6
4	26.0	21.0	3.6	2.4	2.7	28.8	25.9
5	13.0	11.5	3.1	3.7	3.9	13.7	14.1
6	7.6	7.7	3.0	4.8	4.8	14.7	19.1
7	5.3	6.3	2.8	5.9	5.4	15.4	26.1
8	4.4	5.7	2.7	6.6	5.8	26.9	52.2
9	3.4	5.0	2.6	7.5	6.2	18.5	39.1
10	2.9	4.5	2.4	8.4	6.7	20.5	35.1
11	2.5	3.5	2.3	9.1	7.6	23.3	18.7
12	N.D.	2.8	2.1	-	8.6	-	17.8
13	N.D.	2.3	1.9	-	9.5	-	18.1
14	N.D.	1.9	1.6	-	10.3	-	22.7

**Table 5.** Critical frequencies, electron lifetimes and projected velocities for 3C 465 with  $\gamma = 2.2$ 

Distance [']	$\nu_c$ (KP) [GHz]	$\nu_c$ (JP) [GHz]	$H_{\text{eq}}$ [ $\mu\text{G}$ ]	Age(KP) [ $\times 10^7$ yr]	Age(JP) [ $\times 10^7$ yr]	Vel(KP) [100 km s $^{-1}$ ]	Vel(JP) [100 km s $^{-1}$ ]	
N-S	1	>30.0	>30.0	4.5	<1.9	<1.9	>13.7	>13.7
	2	>30.0	>30.0	4.7	<1.8	<1.8	>28.4	>28.4
	3	>30.0	>30.0	5.2	<1.7	<1.7	>46.4	>46.4
	4	26.0	20.9	6.3	1.5	1.7	69.3	62.2
	5	N.D.	N.D.	5.2	-	-	-	-
	6	N.D.	N.D.	4.9	-	-	-	-
	7	N.D.	N.D.	3.8	-	-	-	-
	8	N.D.	N.D.	2.7	-	-	-	-
E-W	1	>30.0	>30.0	5.0	<1.7	<1.7	>14.9	>14.9
	2	>30.0	>30.0	6.5	<1.3	<1.3	>38.5	>38.5
	3	27.9	22.6	7.7	1.2	1.3	67.3	60.5
	4	13.0	11.3	6.2	2.1	2.3	26.1	25.3
	5	5.5	6.5	4.7	4.2	3.9	12.3	16.1
	6	3.5	4.3	3.9	6.1	5.5	14.1	16.3
	7	3.5	3.8	3.4	6.6	6.3	53.8	31.9
	8	4.6	4.4	3.2	5.9	6.0	-	-

The synchrotron loss mechanism for an ensemble of electrons with an initial power-law energy distribution  $N(E)dE \propto E^{-\gamma}dE$  produces a curvature of the originally straight power-law emission spectrum  $I(\nu) \propto \nu^{-\alpha}$ , with  $\alpha = (\gamma - 1)/2$ . The curvature manifests itself at the critical frequency  $\nu_c$ , related to the electron age. The shape of the expected synchrotron spectrum can be computed analytically as a function of the critical frequency, the electron energy distribution index  $\gamma$  and the evolution of the electron pitch-angle distribution with time (Pacholczyk 1970). The model of Kardashev-Pacholczyk (KP) is obtained in the case that electrons maintain the same pitch angle throughout their radiative lifetime (Kardashev 1962). The model of Jaffe-Perola (JP) assumes that there is a redistribution of electron pitch angles on short time scales in comparison with their radiative lifetimes, due to their scattering on magnetic field irregularities (Jaffe & Perola 1973).

We have fitted the spectra of our sources obtained at different distances from the core (see previous section) using both the KP and JP models, since we do not have observational evidence in favour of one of them. We also used different values of the exponent  $\gamma$  of the energy distribution function of the electrons, when no information about this parameter could be obtained from the low-frequency spectrum. The fitting procedure was developed by Murgia & Fanti (1996).

In Fig. 7 we present an example of spectral fits. In Tables 2 to 5 we give the break frequencies obtained from the fitting procedure. The values of the critical frequencies of the KP model have been divided by 4/9 for convenience, for the computation of ages (see next subsection). Typical errors of the break frequencies are of the order of 400 MHz.

We note that in the above analysis, the energy losses due to expansion are not considered. Their effect would be to increase the effect of synchrotron losses, without modifying the shape of the spectrum. In the case of constant expansion rates, the values of the break frequencies would be shifted by the same amount and the differential behaviour of  $\nu_c$  along the sources would be unchanged. However, since low brightness lobes in tailed radio galaxies are likely to be confined by the outer medium (see e.g. Feretti et al. 1992), expansion losses should be negligible.

The results of our spectral fits do not allow us to argue in favour of either the KP or JP model. They are discussed for each source below.

**IC 310** - The low-frequency spectral index of this source up to 2' from the core is  $\alpha_{0.3}^{0.6} \sim 0.4$ . Since we do not expect any effect of self-absorption or ageing in this region we can assume that this spectrum reflects the original energy distribution of the radiating electrons. This implies an index  $\gamma = 1.8$ . The data are well fit with both the KP and the JP models. The break frequencies are given in Table 2.

**NGC 1265** - We fitted the spectra of this source at different distances from the core using flux densities at 4 frequencies (see Fig. 5). The low-frequency spectrum within a few arcmin from the nucleus has a spectral index in the range of 0.4–0.6, therefore only a range for the parameter  $\gamma$  can be inferred. We have used  $\gamma = 1.8, 2.0$ , and 2.2. The value of 1.8 gives a bad fit with both models. Fits with  $\gamma = 2.0$  and  $\gamma = 2.2$  yield good results to both the KP and JP model, but  $\chi^2$  is lower for  $\gamma = 2.2$  (Table 3). The JP model gives a slightly better fit up to 5' from the core,

while the KP model seems more suitable to describe the steepening in the most external region.

**3C 129** - No information is available for this source about the low-frequency spectrum, therefore we fitted our data assuming 4 values of  $\gamma$ : 1.8, 2.0, 2.2, 2.4. The best agreement with the data and the JP and KP models have been obtained using  $\gamma = 2.4$ , which corresponds to an intrinsic spectral index of  $\alpha = 0.7$ . The values of the derived break frequencies are given in Table 4. The KP model gives a slightly better fit for the points within  $7'$  from the core but it is unable to fit the very steep spectrum of the more external points where the JP model fit is significantly better.

**3C 465** - In the innermost source region, the spectral index  $\alpha_{0.6}^{4.8}$  is 0.6, therefore the electron energy index  $\gamma$  is likely to be  $\leq 2.2$ . We fitted the spectra using  $\gamma = 2.0$  and 2.2, and found that the last value gives a better fit (see Table 5). In the innermost points, both the KP and JP models provide a good fit to the spectral data, while at larger distances from the core, the KP model is increasingly better. In the outermost points of the N-S tail, no satisfactory fit to the spectra was found, unless using a different electron energy index. This implies that a simple model of synchrotron emission cannot account for the spectral flattening at high frequency.

#### 4.2. Electron lifetimes and velocities

Synchrotron radiation losses lead to a steepening of the emission spectrum at high frequencies with time. From the value of the critical frequency  $\nu_c$  and of the magnetic field, it is possible to get information on the lifetime of radiating electrons suffering synchrotron and inverse Compton losses against the 3K-background radiation. As the magnetic field strength, we use the equipartition value estimated at different locations along each source. The calculation of the equipartition magnetic field involves a number of assumptions (Pacholczyk 1970). We assume the same volume for relativistic particles and magnetic field (filling factor  $\phi = 1$ ), the same energy in electrons and protons ( $k = 1$ ), and upper and lower cutoff frequencies of 10 MHz and 100 GHz, respectively. The derived values of  $H_{\text{eq}}$  for each source are given in the corresponding table.

The age due to synchrotron plus inverse Compton losses is then expressed by the following relation (Alexander & Leahy 1987):

$$t = 1590 \cdot [\nu_c \cdot (1+z)]^{-0.5} \cdot \frac{H_{\text{eq}}^{0.5}}{H_{\text{eq}}^2 + H_{\text{m}}^2} \text{ Myr} \quad (1)$$

where  $\nu_c$  is the break frequency in GHz,  $H_{\text{eq}}$  is the equipartition magnetic field in  $\mu\text{G}$ , and  $H_{\text{m}} = 3.25 \cdot (1+z)^2$  is the equivalent field strength of the 3K radiation in  $\mu\text{G}$ . We note here that non-uniformities in the particle and field distributions in the sources can complicate the interpretation of the spectral curvature (Wiita & Gopal-Krishna 1990, Eilek & Arendt 1996).

The previous equation is valid for the JP model, where a continuous isotropization of the pitch angle is allowed with time. In the KP model, where particles will maintain their initial pitch-angle over time, the expression for the critical frequency differs from that valid in the JP model by  $\langle \sin^2\theta \rangle^2$ , i.e. 4/9 for an isotropic pitch-angle distribution. Therefore, the right-hand side of Eq. (1) must be divided by 4/9 when using break frequencies obtained in the KP model. To use Eq. (1) also for the KP model, the KP break frequencies in Tables 2 to 5 have been divided by 4/9. The derived ages at different distances from the core for each source are given in Tables 2 to 5 for the two models and are plotted in Fig. 8. Typical errors in lifetimes are of the order of 5%. From the age, we obtained the projected drift velocity of emitting particles at different distances from the core. These are also reported in Tables 2 to 5.

**IC 310** seems to be old, since the electron lifetimes in the outer regions appear to be  $2\text{--}2.5 \times 10^8$  yrs. This is a bit surprising as the source is smaller than the others studied here. This could suggest the existence of strong projection effects, but this is in contrast with the low velocity ( $180 \text{ km s}^{-1}$ ) of IC 310 with respect to the Perseus cluster. We note that the radio structure shows no evidence of any transverse expansion. This suggests that the source is well confined by the external medium and that electrons have not suffered significant expansion losses, and can thus survive for such a long time. The projected velocity of radiating electrons decreases along the tail from  $\sim 900 \text{ km/s}$  to  $\sim 200 \text{ km/s}$ . Projection effects would increase these values. Miley (1973) pointed out that the radio plasma of IC 310, being  $\sim 10$  times less luminous than NGC 1265, may have been ejected with less kinetic energy. This may comply with the relatively low drift velocity inferred for its tail.

**NGC 1265** reaches an age of  $6.7 \times 10^7$  yr. The average electron velocity is  $\sim 3000 \text{ km/s}$ , and increases with distance, up to  $7'$  from the core. The radial velocity of this galaxy with respect to the Perseus cluster is  $2055 \text{ km s}^{-1}$ . We note that O'Dea & Owen (1987) argued, based on the magnetic field in the jets, that NGC 1265 should be within  $45^\circ$  of the plane of the sky. If this is the case the total galaxy velocity would be consistent with the average value estimated from spectral aging.

**3C 129** is  $\sim 10^8$  yrs old in the more external regions. We remember that for the outer regions of this source only the JP model is able to fit the spectral index data. The particle velocity is around  $2000 \text{ km/s}$ , showing variations along the tail. It seems that there is an increase of velocity at about  $6'\text{--}7'$  from the core, where a large bend in the radio structure occurs.

In **3C 465** the particle lifetimes in the E-W lobe reach  $6\text{--}6.5 \times 10^7$  yrs and the average velocity of emitting electrons is  $\sim 3500 \text{ km/s}$ . The velocity decreases at  $4'\text{--}6'$  from the core, then it increases in the outermost source regions. In the N-S tail, the points where the break frequencies have been estimated are too few to derive the trend of

electron age and velocity. The velocity implied at 4' from the nucleus is about 6500 km s<sup>-1</sup>.

The ages obtained for the present galaxies are of the same order as in other objects for which similar studies were made, such as 3C 31, 3C 449 (Andernach et al. 1992), and NGC 4869 (Feretti et al. 1990). The relativistic electron velocities are higher than expected, as we would expect that the particles diffuse at the typical sound speed (some hundred km s<sup>-1</sup>) or that their motion reflects the proper motion of the parent galaxy within the cluster, as in NGC 1265. We note that there could be a selection effect, in that tailed radio sources with very long tails may be those associated with cluster galaxies with high proper motion. However, in all cases we detect significant local variations, with values up to 5000–6000 km s<sup>-1</sup>, at large distance from the core. The inferred trends could be explained by: a) projection effects, b) the existence of reacceleration processes, which allow the electrons to extend their lifetimes, c) the presence of bulk streaming motions in the radio-emitting plasma. The existence of bulk streaming motions in radio galaxies has been suggested by Liu et al. (1989), on the basis of similar electron ageing arguments. We have also considered the possibility that the magnetic field, which enters in the computation of the age, is not the equipartition value. We have noted, however, that the equipartition magnetic fields in these sources are always close to the values which give the maximum lifetimes (Van der Laan & Perola 1969), therefore the use of significantly different values of the magnetic field would make the velocities still higher.

#### 4.3. Polarization properties

We have determined the linear polarization in all sources at 10.6 GHz, and at 4.8 GHz, and 2.7 GHz (when available). The degree of polarization generally increases along the tail, reaching values larger than 50% at 10.6 GHz. Towards the head, the degrees of polarization is lower, owing to beam depolarization within the regions where the twin jets (and hence the magnetic fields tied to them) get strongly bent backwards. For the same reason, the measured fractional polarization can also be significantly lower at the longer wavelengths. Synchrotron radiation theory predicts that the intrinsic polarization percentage is given by

$$P_{\text{intr}} = \frac{3\alpha + 3}{3\alpha + 5} \quad (2)$$

where  $\alpha$  is the observed emission spectral index. At the tail's end the spectral index typically increases to  $\alpha \sim 2$ ; then the intrinsic fractional polarization expected there is  $\sim 80\%$ . The observed polarization percentage is related to the intrinsic theoretical one by the expression

$$P_{\text{obs}} = P_{\text{intr}} \frac{H_o^2}{H_o^2 + H_r^2} \quad (3)$$

where  $H_o$  and  $H_r$  are the ordered and random component of the magnetic field, respectively. The high linear polarization percentage seen at 10.6 GHz implies a high, though not complete, degree of ordering of the magnetic field. The increase of the polarization percentage with distance from the core is much stronger than that expected from the spectral index variation (Eq. 2). Therefore, the degree of ordering of the magnetic field is higher as the radio emitting plasma is getting older. In 3C 129, the degree of polarization at the tail's end is close to the theoretical value. We derive that 91% of the magnetic field in this region is ordered on a scale of  $\sim 20$  kpc. At  $\sim 5'$  from the core, the ordered component of the magnetic field is  $\sim 65\%$ . In the other sources, the uniform component of the magnetic field is  $\sim 70\text{--}75\%$  at the tails' ends on a 20–30 kpc scale. If the increase in the ordering of the magnetic field is due to reconnection of the magnetic field (e.g. Soker & Sarazin 1990), then this would be accompanied by energy release which could also be responsible for reaccelerating the electrons.

In all sources, the magnetic field is aligned with the tails. This alignment has been interpreted as due to the anisotropic effect of ram pressure (Pacholczyk & Scott 1976) and is consistent with the increase of magnetic field ordering along the tails.

## 5. Conclusions

We have presented a multi-frequency study of 4 tailed radio galaxies. The results are summarized in the following.

Point-to-point spectra using 3 or 4 frequencies, in the range from 327 MHz to 10.6 GHz, have been obtained along the tails, up to the outermost regions. We find that the spectrum in each radio galaxy progressively steepens with distance from the core, and at each location it is steeper at higher frequencies. Except for the N-S tail of 3C 465, the spectra are well fitted by models involving synchrotron energy losses, assuming both that the electron pitch angle is constant over time (KP model), and that there is continuous isotropization of the pitch-angle distribution (JP model). The spectral fits do not allow us to argue in favour of either the KP or JP model. The critical frequency obtained by spectral fits decreases with increasing distance from the core. Assuming that the magnetic field is at the equipartition value, we show that the lifetimes of radiating electrons after synchrotron and Inverse Compton losses are generally between  $10^7$  and  $10^8$  yr, with the exception of IC 310 where the electrons in the outer tail are older than  $10^8$  yr. Electron drift velocities are generally larger than 2000 km/s, and show significant variations along the tails. This implies that reacceleration processes or bulk motions should be present.

The polarization data at 10.6 GHz indicate that in all the sources the magnetic fields are oriented along the tails. The polarization percentage increases along the tails, reaching values of  $\simeq 50\%$ . In 3C 129 the polarization per-

centage in the outermost regions is  $\sim 75\%$ , close to the theoretical synchrotron value. The degree of ordering of the magnetic field increases along the tails, viz. up to  $\sim 75\%$  in IC 310, NGC 1265, and 3C 465. In 3C 129 the ordered component of the magnetic field exceeds 90% at the tail's end.

*Acknowledgements.* We thank Matteo Murgia for his help in the application of the code for the spectral fits. We are grateful to the referee, Chris O'Dea, for helpful suggestions. Part of this work was supported by the Deutsche Forschungsgemeinschaft, grant KL533/4-2 and by European Commission, TMR Programme, Research Network Contract ERBFMRXCT97-0034 "CERES".

## References

- Alexander P., Leahy J.P., 1987, MNRAS 225, 1  
 Andernach H., Feretti L., Giovannini G. et al. 1992, A&AS 93, 331  
 Baars J.W.M., Genzel R., Pauliny-Toth I.I.K., Witzel A., 1977, A&A 61, 99  
 Burns J.O., Sulkanen M.E., Gisler G.R., Perley R.A., 1992, ApJ 388, L49  
 Carilli C.L., Perley R.A., Dreher J.W., Leahy J.P., 1991, ApJ 383, 554  
 Eilek J.A., Burns J.O., O'Dea C.P., Owen F.N., 1984, ApJ 278, 37  
 Eilek, J.A., Arendt, P.N., 1996, ApJ 457, 105  
 Emerson D.T., Klein U., Haslam C.G.T., 1979, A&A 76, 92  
 Feretti L., Dallacasa D., Giovannini G., Venturi T., 1990, A&A 232, 337  
 Feretti, L., Perola, G.C., Fanti, R., 1992, A&A 265, 9  
 Gisler G.R., Miley G.K., 1979, A&A 76, 109  
 Jaffe W.J., Perola G.C., 1973, A&A 26, 423  
 Jägers, W.J., 1987, A&AS 71, 603  
 Leahy, J.P., 1984, MNRAS 208, 323  
 Kardashev N.S., 1962, Sov. Astron. AJ 6, 317  
 Klein, U., Mack, K.-H., 1995, in *Multifeed Systems for Radio Telescopes*, D.T. Emerson & J.M. Payne Eds., ASP Conference Series, Vol. 75, p. 318  
 Liu R., Riley J., Warner P., Pooley G., Alexander P., 1989, MNRAS 240, 501  
 Mack K.-H., Feretti L., Giovannini G., Klein U., 1993, A&A 280, 63  
 Miley G.K., 1973, A&A 26, 413  
 Murgia M., Fanti R., 1996, Internal Technical Report IRA 228/96  
 O'Dea, C.P., Owen, F.N., 1987, ApJ 316, 95  
 Pacholczyk A.G., 1970, Radio Astrophysics, Freeman, San Francisco  
 Pacholczyk A.G., Scott J.C., 1976, ApJ 203, 313  
 Rudnick L., Burns J.O., 1981, ApJ 246, L69  
 Sijbring L.G., 1993, Ph.D. thesis, Univ. Groningen  
 Soker, N., Sarazin, C.L., 1990, ApJ 348, 73  
 Van Breugel W., 1982, A&A 110, 225  
 Van Breugel W., Jägers W., 1982, A&AS 49, 529  
 Van der Laan, H., Perola, G.C., 1969, A&A 3, 468  
 Wiita, P.J., Gopal-Krishna, 1990, ApJ 353, 476

This article was processed by the author using Springer-Verlag L<sup>A</sup>T<sub>E</sub>X A&A style file L-AA version 3.



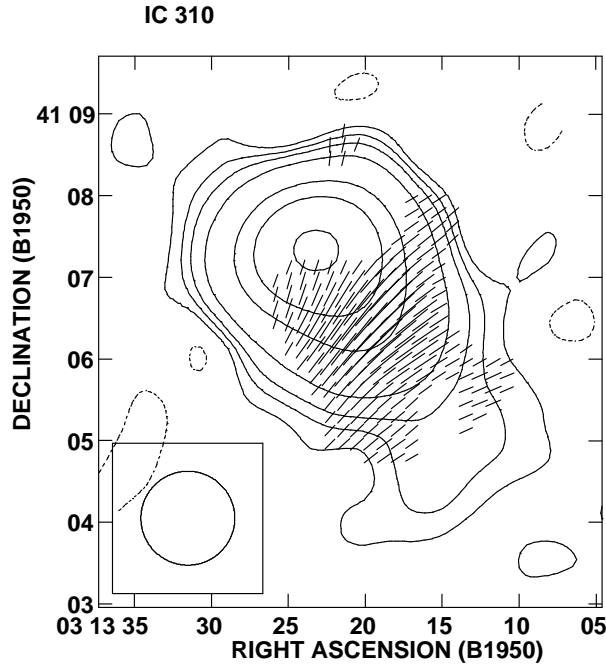


**Fig. 1.** Contour map of IC 310 at 10.6 GHz. Superimposed lines represent the orientation of the polarization vector and are proportional in length to the polarized intensity ( $1'' = 0.1$  mJy/beam). Contour levels are: -1, 1.5, 3, 5, 10, 30, 50, 90 mJy/beam.

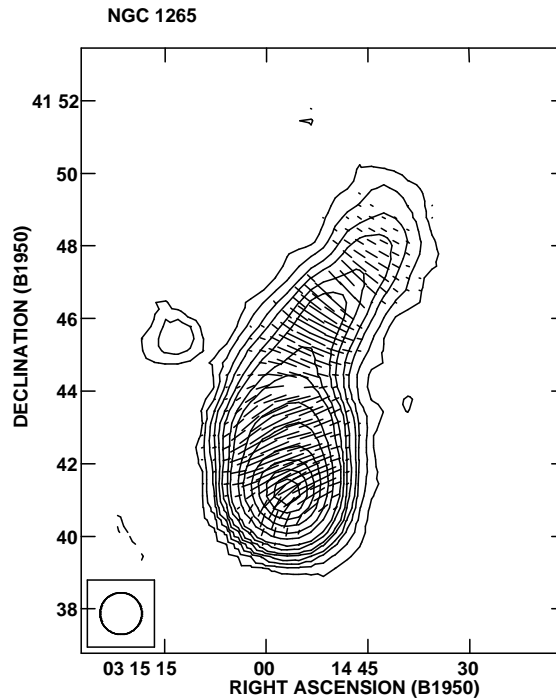


**Fig. 2.** Contour map of NGC 1265 at 10.6 GHz. The peak to S-E of the source in the 2.7 GHz image is the unrelated background source 3C 83.1A. The polarization vector and are proportional in length to the polarized intensity, with  $1'' = 0.25$  mJy/beam. Contours levels are as follows: 2, 4, 7, 10, 15, 20, 30, 40, 70, 100, 150, 200, 250, 300 mJy/beam.

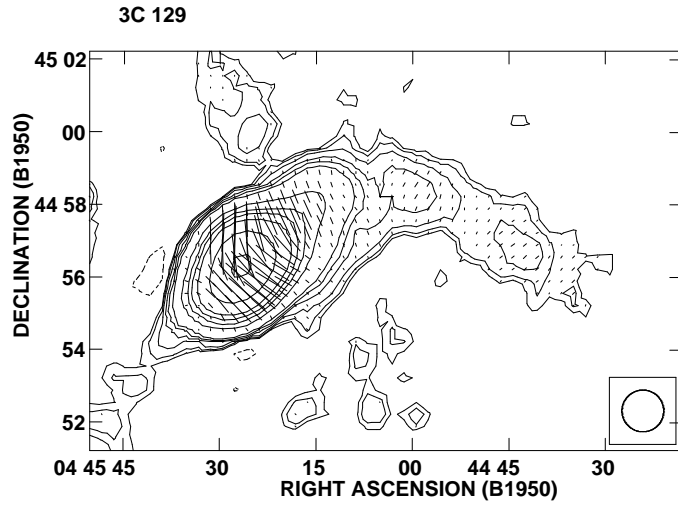


**Fig. 3.** Contour map of 3C 129 at 10.6 GHz. Superimposed lines represent the orientation of the polarization vector and are proportional in length to the polarized intensity, with  $1'' = 0.3$  mJy/beam. Contour levels are: -1.5, 1.5, 2, 3, 5, 7, 10, 30, 50, 70, 100, 200, 400 mJy/beam.

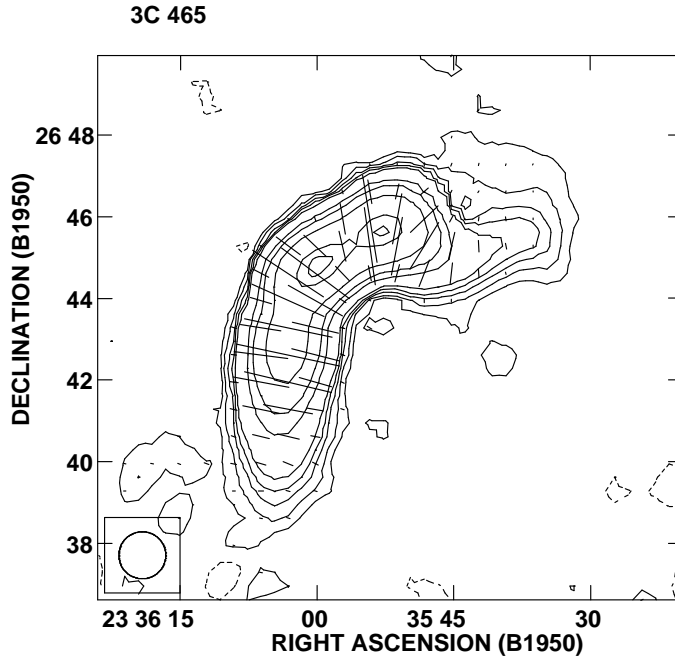


**Fig. 4.** Contour map of 3C 465 at 10.6 GHz. The polarization vectors are proportional in length to the polarized intensity, with  $1'' = 0.3$  mJy/beam. Contour levels are as follows: -1.5, 1.5, 3, 5, 7, 10, 30, 50, 100, 250, 300 mJy/beam.

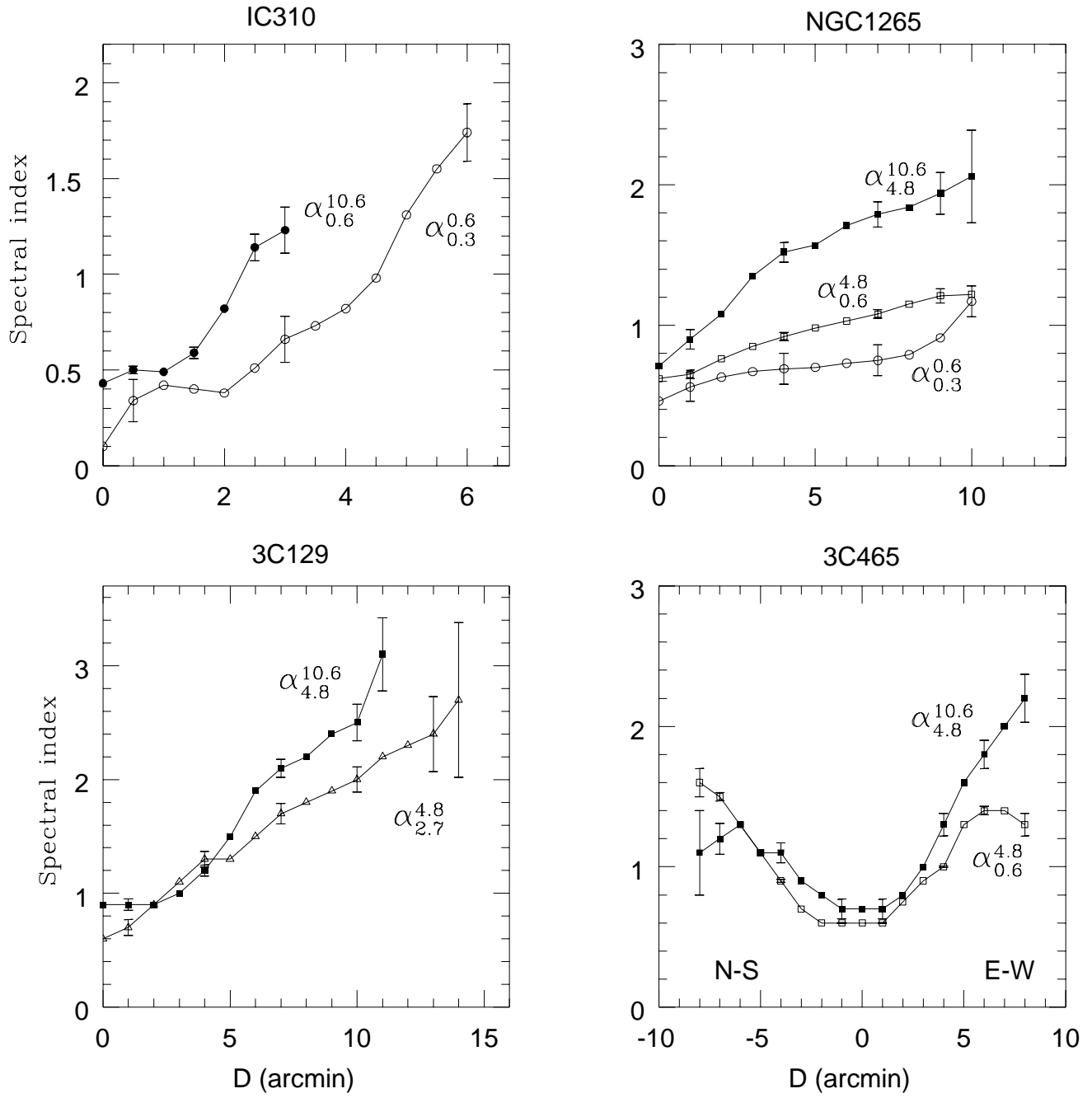


**Fig. 5.** Trend of the spectral index of the sources under study along the ridge of maximum brightness.

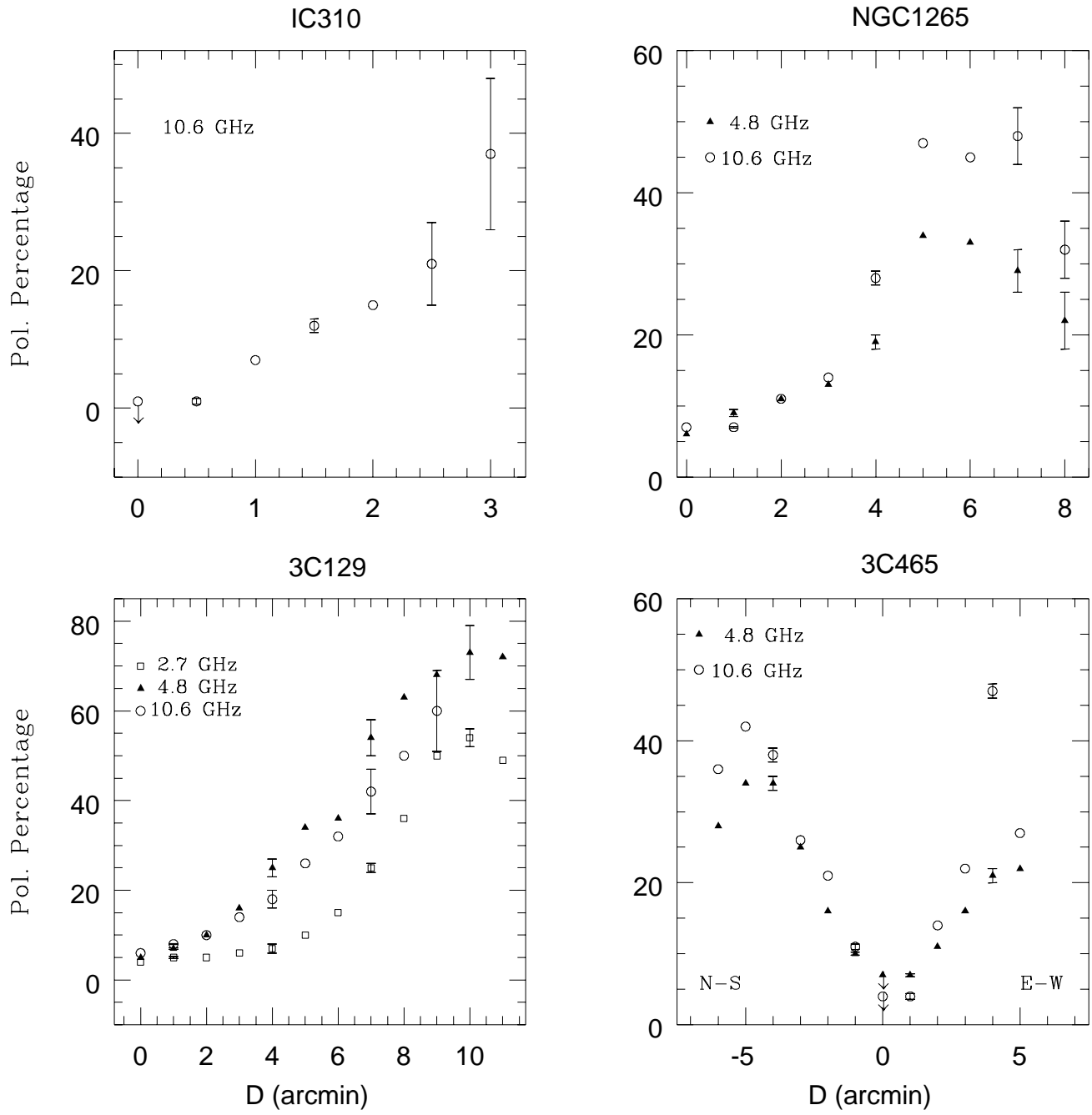


**Fig. 6.** Polarization percentage of the sources under study along the ridge of maximum brightness.

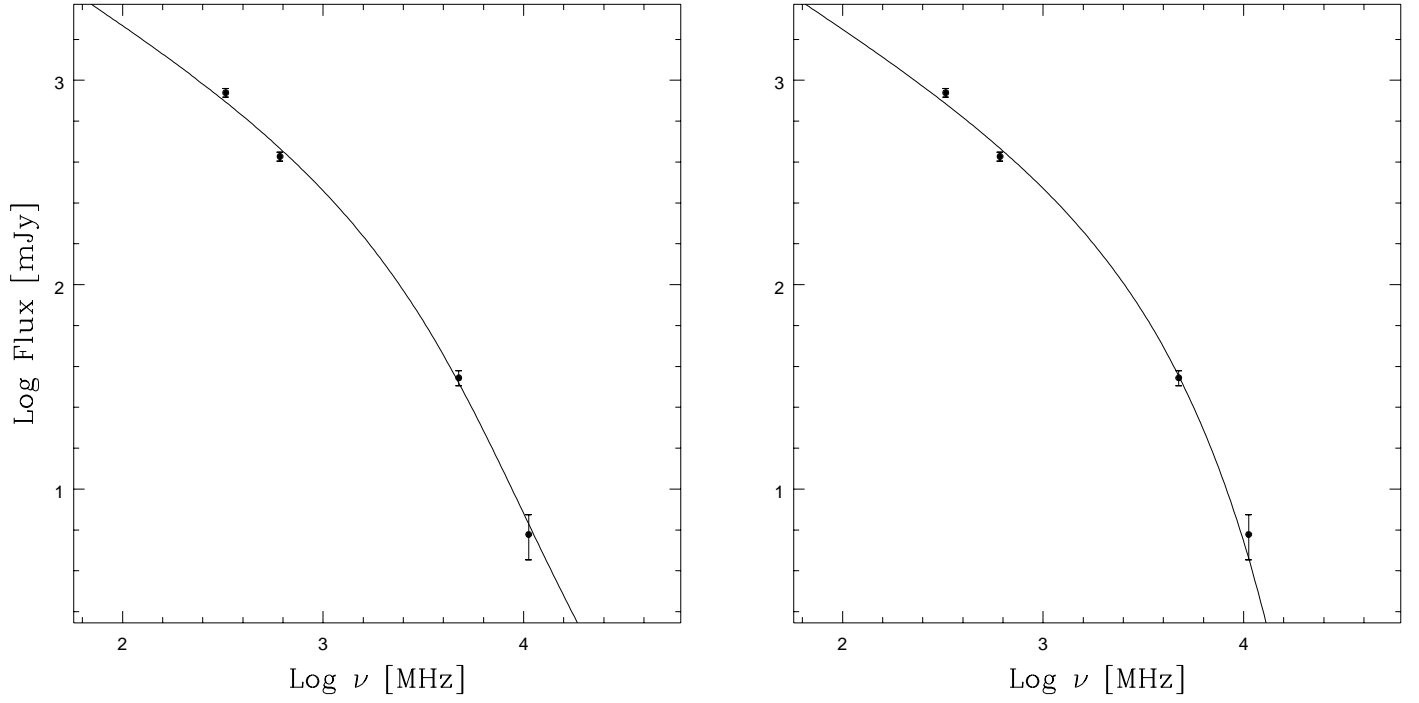


**Fig. 7.** Examples of the fit to the spectrum of NGC 1265 at 10' from the core. The continuous line represents the best fit model, obtained with  $\gamma = 2.2$ . The left and right panels refer to the KP and JP model, respectively.

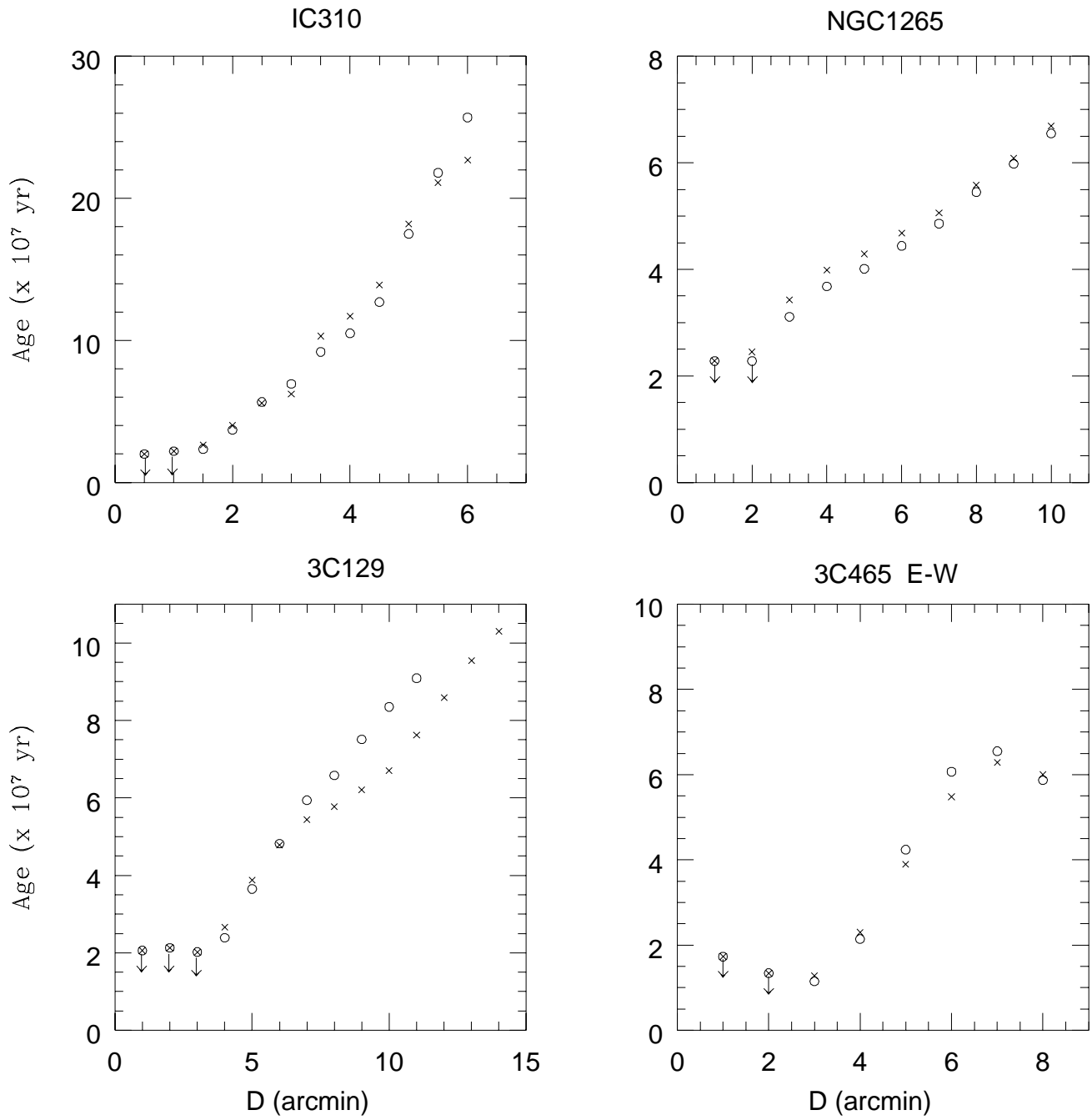


**Fig. 8.** Plots of the radiating electron lifetimes at different distance from the core. The open circles and crosses refer to the Kardashev-Pacholczyk and Jaffe-Perola model, respectively.